

MEASUREMENT OF LOW WAVE NUMBER
COMPONENTS OF WALL PRESSURE
BENEATH A PLANE TURBULENT
BOUNDARY LAYER

John Karl Morris

MEASUREMENT OF LOW WAVE NUMBER COMPONENTS
OF WALL PRESSURE
BENEATH A PLANE TURBULENT BOUNDARY LAYER

by

Lieutenant Commander JOHN K. MORRIS, USN

S.B., United States Naval Academy

1961

SUBMITTED IN PARTIAL FULFILLMENT

OF THE REQUIREMENTS FOR THE

DEGREE OF OCEAN ENGINEER

AND

MASTER OF SCIENCE

IN NAVAL ARCHITECTURE AND MARINE ENGINEERING

at the

MASSACHUSETTS INSTITUTE OF TECHNOLOGY

June, 1973

MEASUREMENT OF LOW WAVE NUMBER COMPONENTS
OF WALL PRESSURE
BENEATH A PLANE TURBULENT BOUNDARY LAYER

by

Lieutenant Commander JOHN K. MORRIS, USN

Submitted to the Department of Ocean Engineering on May 11, 1973, in partial fulfillment of the requirements for the degree of Ocean Engineer and Master of Science in Naval Architecture and Marine Engineering.

ABSTRACT

The suitability of a rectangular membrane for use as a low wave number filter is investigated. The membrane is flush mounted beneath a plane turbulent boundary layer and its displacement spectral density determined. The low wave number wall pressure spectral density is analytically determined from the membrane displacement spectral density.

Thesis Supervisor: Patrick Leehey
Title: Professor of Ocean Engineering

ACKNOWLEDGEMENT

The author wishes to acknowledge the assistance of all those members of the Institute whose efforts contributed towards making this project possible.

In particular, I wish to express my special thanks to two people for their inspiration and near infinite patience: Professor Patrick Leehey and my wife.

TABLE OF CONTENTS

	<u>Page</u>
Title Page	1
Abstract	2
Acknowledgement	3
Table of Contents	4
List of Figures	5
Nomenclature	6
I INTRODUCTION	7
II EXPERIMENTAL PROCEDURES	10
III EXPERIMENTAL RESULTS	15
IV DISCUSSION OF RESULTS	21
V CONCLUSIONS	23
VI RECOMMENDATIONS	24
References	26
APPENDIX I	38
APPENDIX II	42
APPENDIX III	44

LIST OF FIGURES

<u>Figure</u>		<u>Page</u>
1	Membrane Mounting Details	27
2	Membrane Displacement Spectral Density Measurement Equipment Schematic	29
3	Membrane Acoustic Excitation Response Measurement Equipment Schematic	30
4	Apparent Membrane Wave Speed versus Frequency	31
5	Membrane Dampening at Resonant Points	32
6	Membrane Displacement Spectral Density Response to Plane Turbulent Boundary Layer Excitation	33
7	Membrane Displacement Spectral Density Response to Acoustic Excitation and Response to Plane Turbulent Boundary Layer Excitation	34
8	Data Coordinate System	35
9	Low Wave Number Pressure Spectral Density Isogram	36
10	Low Wave Number Pressure Spectral Density Response Contour	37

NOMENCLATURE

6

$A_n(k)$	Lateral shape function
$C(l,k,K)$	Fourier transform of longitudinal factor of membrane's Green's function
T_m	Uniform membrane tension
c_o	Velocity of sound in air
c_m	Velocity of waves in membrane
$f_{m,n}$	Resonant frequency of (m,n) membrane mode
l_1	Longitudinal membrane dimension
l_3	Transverse membrane dimension
q	Free stream dynamic head, $\frac{1}{2} \rho U_\infty^2$
U_∞	Free stream velocity
Φ	Autocorrelation function
β	Membrane decay rate
δ	Dirac- δ function
δ^*	Displacement thickness
η	Dampening factor
λ_3	Lateral integral correlation length of exciting wall pressure
ν	Kinematic viscosity
σ_{am}	Membrane added mass
σ_m	Membrane surface density
σ_t	Membrane total surface density
ϕ_d	Membrane displacement spectral density
ϕ_p	Boundary layer pressure spectral density
$\bar{\phi}_p$	Non-dimensionalized pressure spectral density
$\omega_{m,n}$	Angular resonant frequency of (m,n) mode

CHAPTER I

INTRODUCTION

Mobile sonar systems are subject to self-noise induced by turbulent boundary layer wall pressure fluctuations. These boundary layer pressure fluctuations may be subdivided into convective components and low wave number components. The low wave number component is of particular importance to sonar applications because of the low free stream velocity and the relatively high frequencies of interest. Under these conditions, low wave number components (well separated from the convective components) may be dominant contributors to self-noise.

This study deals with the experimental determination of low wave number wall pressure statistics. The existing data on wall pressure statistics has largely been determined by measuring pressure fluctuations with pairs of flush-mounted microphones. This spectra is dominated by the convective components and therefore serves poorly to determine the low wave number components. Low wave number contributors have been investigated, and the following techniques for wave number filtering have been considered:

1. Line array of flush-mounted transducers.
2. Modal excitation of tensioned, clamped bars.
3. Modal excitation of plates.
4. Modal excitation of membranes.

Line array filters have been suggested and used by Maidanik and Jorgensen (1), Blake and Chase (2), and Jameson (3). While this is potentially an excellent approach, cost, fabrication, and signal processing difficulties have been encountered. Published data based on this technique is limited to estimates of the upper bound of the low wave number contribution.

Aupperle and Lambert (4) have performed the theoretical analysis for clamped bars under tension, but no test results have been published. Jameson has investigated the use of plates as low wave number filters, and provided preliminary results at the 85th Meeting of the American Acoustical Society in April, 1973.

The use of membranes will avoid the dispersive nature of bars and plates, as well as the surface discontinuities in bars and the inexact boundary conditions obtainable with plates. For these reasons, a rectangular membrane was selected as a low wave number filter. The membrane, under uniform tension, was flush-mounted beneath a plane turbulent boundary layer. The membrane was elongated in the direction of flow such that only the lowest lateral mode would be excited over the frequency range of interest. Measurements were made in the low noise, low turbulence wind tunnel, described in detail by Hanson (5). This is the same tunnel used by Blake (6) and Burton (7) in their wall pressure measurements.

The analytic background for these measurements was performed by Leehey and Davies (8). From their analysis it can be deduced that the normal displacement spectral density, $\phi_d(\omega)$, at the midpoint of the membrane is related to wall pressure wave number spectral density, $\phi_p(\bar{k}, \omega)$, by the following relationship:

$$\phi_d(\omega) = \frac{1}{(\sigma_t c^2)^2} \sum_{n=1}^{\infty} \sin^2\left(\frac{n\pi}{2}\right) \int_{-\infty}^{\infty} \int_{-\infty}^{\infty} |A_n(k_x)|^2 |C(l, k_x, k_n(\omega))|^2 \phi_p(\bar{k}, \omega) d\bar{k} \quad (1)$$

Assuming negligent contribution from higher lateral modes, and other constraints as specified in Appendix I, this expression can be approximated by the following relationship when evaluated at resonant frequencies $\omega_{m,1}$:

$$\phi_d(\omega_{m,1}) \cong \frac{1}{2} \cdot \frac{l_3}{l_1} \left[\frac{\pi}{\sigma_t \cdot \beta \cdot \omega_{m,1}} \right]^2 \cdot \left[\phi_p(k_m, 0, \omega_{m,1}) + \phi_p(-k_m, 0, \omega_{m,1}) \right] \quad (2)$$

When the conditions have been met which permit the use of Equation (2), the value of ϕ_p can be evaluated as a function of the experimentally determined values of ϕ_d , β , and σ_t .

CHAPTER II

EXPERIMENTAL PROCEDURE

The object of the experiment was to obtain directly the values of displacement spectral density, ϕ_d , membrane resonant dampening β , and modal surface density σ_t , for use in calculating pressure spectral density, ϕ_p . In addition, the membrane response to acoustic excitation simulating wind tunnel acoustic flow noise was desired.

Membrane Preparation. The rectangular membrane was fabricated in the following manner. A twenty-eight inch diameter mylar (polyethylene terephthalate) bass drum head was uniformly tensioned on a bass drum frame. The uniformity of the tension was determined by exciting the circular mylar membrane acoustically with pure tones at its resonant frequencies. The resultant Chladni patterns were observed using a light dusting of fine sand to identify nodes. With uniform tension achieved, a backing plate of 3/4 inch plywood was cemented to the lower surface of the mylar membrane. This backing plate contained a plexiglass edged, rectangular shaped cut-out which served to define the desired wave filter membrane. The membrane so defined had the following characteristics:

1. Dimensions: $l_1 = 0.55$ m, $l_3 = 0.05$ m
2. Thickness: 8.5 mils
3. Surface density: 0.292 Kg/m²

Plexiglass edges were used to insure a sharply defined boundary for the wave filter membrane. The backed membrane, still held by the tensioning frame, was set in a mounting frame and then flush-mounted in the wind tunnel test section, forming the lower panel of the test section. The wave filter was oriented such that the centerline of its long dimension (l_1) coincided with the vertical plane of the test section centerline, parallel to the mean flow path. Membrane mounting details and position relative to the test section are shown in Figures 1-a and 1-b respectively.

With the membrane secured in position in the wind tunnel, acoustic excitation and sand were used to observe the Chladni patterns of the rectangular membrane. It was from these observations that modal resonant frequency response could be correlated to specific modes.

Membrane Characteristics. The only membrane characteristic explicitly required for the solution of Equation (2) is σ_t , where

$$\sigma_t = \sigma_m + \sigma_{am} \quad (3)$$

In order to determine σ_t , however, the membrane tension must be accurately known. By measuring the frequency at which the resonant modes occur, the relationship between $f_{m,n}$ and $\sqrt{T_m/\sigma_t}$ can be determined from the following

equation by Morse (9):

$$f_{m,n} = \frac{1}{2} \cdot \sqrt{T_m/\sigma_t} \cdot \sqrt{(m/l_1)^2 + (n/l_3)^2} \quad (4)$$

Because σ_{am} is strongly frequency dependent, the value of $\sqrt{T_m/\sigma_t}$ is expected to asymptotically approach $\sqrt{T_m/\sigma_m}$ (the in vacuo membrane wave speed) at high frequencies.

The value of σ_m is determined by weighing a sample of the membrane material of known surface area. Based on the estimated asymptotic value of membrane wave speed and the measured value of σ_m , the tension, T_m , is defined. By back substitution of T_m in Equation (4), the value of σ_t at each of the resonant modes can be calculated.

Resonant Frequency Dampening. Modal dampening measurements were made using the following techniques:

1. Measuring bandwidth of resonant response peaks at the 3 dB down point.
2. Measuring membrane displacement decay after "impulse" excitation induced by tapping the membrane, both with and without wind tunnel flow.
3. Calculation of dampening losses assuming dampening due to acoustic radiation.

Dampening measurements were also attempted by acoustically exciting the membrane with either pure tones or white noise and measuring the decay response. The relatively long re-

reverberation time of the test section chamber, however, precluded accurate measurements using this technique.

Boundary Layer Excitation. Turbulent boundary layer excitation was induced by a series of wind tunnel duct flows varying from 12 m/sec to 28 m/sec. Additional measurements were taken at 38 m/sec and 50 m/sec to permit increased correlation with data obtained by Blake (6). Membrane response in the form of center displacement spectral density was obtained using a non-contact, optical displacement gage. An equipment arrangement schematic of the measuring and analyzing devices is shown in Figure 2. Reference displacement spectral density of the backing plate and membrane were measured at minimum and maximum tunnel speeds (12 m/sec and 50 m/sec).

Response to Acoustic Excitation. The membrane displacement response to simulated tunnel acoustical flow induced excitation was measured as shown schematically in Figure 3. Based on the analysis described in Appendix II, the flow induced acoustic noise can be determined by knowing turbulent boundary layer wall pressure fluctuations and the tunnel response to acoustic excitation. Boundary layer excitation measurements were made at 28 m/sec to conform to test section sound pressure level information available. No-flow acoustic excitation was made using a broad-band "white noise" source in series with a wave shap-

ing filter network. One-third octave averaged sound pressure levels were used over the range of 800 to 2000 Hz, that band for which reliable acoustic data is available currently for this tunnel.

CHAPTER III

EXPERIMENTAL RESULTS

Membrane Characteristics. The frequency of modes (7,1) through (19,1) were obtained using acoustic excitation and observing the Chladni patterns. The frequency of modes (5,1) through (27,1) were obtained from spectral density plots obtained using boundary layer excitation. The results of these two observations are shown in Table 1.

TABLE 1

Measured Values of Modal Resonant Frequencies (frequency in Hz)		
(m,n)	Chladni	ϕ_d
1,1	-	-
3,1	-	-
5,1	-	1375
7,1	1570	1550
9,1	1789	1765
11,1	1965	1975
13,1	2177	2200
15,1	2410	2435
17,1	2644	2685
19,1	2907	2925
21,1	-	3185
23,1	-	3440
25,1	-	3715
27,1	-	3980

Based upon the calculated values of $\sqrt{T_m/\sigma_t}$ (using the ϕ_d values of modal frequency) the membrane wave speed appears to asymptotically approach 150 m/sec.

Apparent membrane wave speed versus frequency is shown in Figure 4. The asymptotic value of $\sqrt{T_m/\sigma_t}$ yields a membrane tension of 6570 new/m. Based on this value of tension, the values of σ_{am} for modes (5,1) through (19,1) were calculated and are presented in Table 2.

TABLE 2

Measured Values of Modal Added Mass Effect for $\sigma_m = 0.292 \text{ Kg/m}^2$		
Mode	$f_{m,n}$ (Hz)	σ_{am} Measured (Kg/m ²)
(5,1)	1375	0.1166
(7,1)	1550	0.0840
(9,1)	1765	0.0539
(11,1)	1975	0.0401
(13,1)	2200	0.0296
(15,1)	2435	0.0219
(17,1)	2685	0.0146
(19,1)	2925	0.0121

Resonant Frequency Dampening. Modal dampening was calculated as specified in Chapter II. Experimental methods show good agreement in both absolute magnitude and frequency dependence. This data is presented graphically in Figure 5. Analytic values determined assuming all dampening is due to radiated acoustic losses are also shown in Figure 5.

Response to Acoustic Excitation. Figure 7 shows the

membrane displacement spectral density under boundary layer excitation at 29 m/sec, and the no-flow acoustical excitation displacement response of the membrane. Turbulent boundary layer excitation response is consistently greater than acoustic excitation response over the range measured. No phase relationship between flow and acoustic excitation was determined, nor was longitudinal acoustic mode orientation of the simulated or actual acoustic flow noise known.

Boundary Layer Excitation. Displacement spectral density for odd modes of the rectangular membrane's response to plane turbulent boundary layer excitation was determined for various flow rates. Under high flow rates (greater than 28 m/sec) the membrane showed strong resonant peaks beginning with the (5,1) mode and continuing through the (27,1) mode; and weak but recognizable resonant peaks for the (1,1) and (3,1) modes. In order to reduce strong resonant excitation response of the membrane backing plate (which masked the lower membrane modes) it was found necessary to modify the original membrane backing plate by the addition of 1/4 inch lead sheath as shown in Figure 1-a. The addition of the lead provided approximately a 10 dB decrease in backing plate vertical acceleration and shifted much of the resonant activity in the plate below the (1,1) membrane frequency.

For test section flow rates greater than 20 m/sec, the turbulent boundary excitation produced well defined resonant responses, see Figure 6. For flows greater than 25 m/sec, modes (5,1) to (11,1) show resonant peaks greater than 10 dB above the 12 m/sec base line response. The presence or absence of higher order even transverse modes was not determined due to the centerline placement of the sensor.

Pressure Spectral Density. Calculated pressure spectral density, non-dimensionalized on $U_\infty/q^2\delta^*2$, is presented in Table 3. Table 4 contains values of $\omega\delta^*/U_\infty$ and $k_1\delta^*$ for the corresponding values of $\overline{\delta}_p$ in Table 3. Values of δ^* for wind tunnel velocities of 15.7 m/sec and 19 m/sec were extrapolated from the data by Blake (6) by assuming that:

$$\delta^* = \text{Constant}(x) \cdot (U_\infty \cdot x / \nu)^{-\frac{1}{5}}$$

where "x" is taken to be 88 inches (virtual origin of the boundary layer), leading to a value of 0.07 for the constant.

Figure 8 describes a three dimensional coordinate system which maps values of $10 \log_{10}(\overline{\delta}_p)$ above the $k_1\delta^*$, $\omega\delta^*/U_\infty$ plane. Figure 9 shows an isogram of $10 \log_{10}(\overline{\delta}_p)$ obtained by passing a plane of constant $\overline{\delta}_p$ through the response space curve. Figure 10 shows the three dimensional data field collapsed onto the $k_1\delta^*$, $\omega\delta^*/U_\infty$ plane. Response contours are indicated with respect to the convective ridge ($\omega\delta^*/U_\infty \approx 0.7k_1\delta^*$).

TABLE 3

Mode (m,n)	$f_{m,n}$ (Hz)	$10 \log_{10} \left\{ \frac{\phi_p(k_1, 0, \omega) + \phi_p(-k_1, 0, \omega) U_\infty}{q^2 f^* 2} \right\}$							
		15.7 m/sec	19 m/sec	24 m/sec	26.5 m/sec	29 m/sec	38 m/sec	50 m/sec	
(5,1)	1375	-75	-75	-75	-74	-74	-	-	
(7,1)	1550	-76	-76	-77	-76	-75	-72	-68	
(9,1)	1765	-77	-77	-78	-78	-77	-72	-68	
(11,1)	1975	-	-80	-82	-81	-81	-78	-74	
(13,1)	2200	-	-79	-81	-81	-82	-79	-77	
(15,1)	2435	-	-	-81	-81	-81	-80	-78	
(17,1)	2685	-	-	-81	-82	-81	-80	-78	
(19,1)	2925	-	-	-79	-79	-79	-78	-77	

TABLE 4

Mode (m,n)	$f_{m,n}$ (Hz)	Wind Tunnel Velocity															
		15.7 m/sec		19 m/sec		24 m/sec		26.5 m/sec		29 m/sec		38 m/sec					
		$\frac{\omega f^*}{U_\infty}$	$\frac{U_\infty}{q 2 f^* 2}$	$\frac{\omega f^*}{U_\infty}$	$\frac{U_\infty}{q 2 f^* 2}$	$\frac{\omega f^*}{U_\infty}$	$\frac{U_\infty}{q 2 f^* 2}$	$\frac{\omega f^*}{U_\infty}$	$\frac{U_\infty}{q 2 f^* 2}$	$\frac{\omega f^*}{U_\infty}$	$\frac{U_\infty}{q 2 f^* 2}$	$\frac{\omega f^*}{U_\infty}$	$\frac{U_\infty}{q 2 f^* 2}$	$\frac{\omega f^*}{U_\infty}$	$\frac{U_\infty}{q 2 f^* 2}$		
(5,1)	1375	4.62	0.24	3.68	0.23	2.69	0.21	2.41	0.21	2.16	0.21	1.63	0.21				
(7,1)	1550	5.21	0.34	4.15	0.32	3.03	0.30	2.72	0.30	2.43	0.29	1.84	0.29				
(9,1)	1765	5.93	0.43	4.72	0.42	3.45	0.38	3.09	0.38	2.77	0.37	2.10	0.37				
(11,1)	1975	6.64	0.53	5.29	0.51	3.86	0.47	3.46	0.46	3.10	0.45	2.35	0.45				
(13,1)	2200	7.39	0.62	5.89	0.60	4.30	0.55	3.85	0.55	3.45	0.54	2.61	0.53				
(15,1)	2435	8.15	0.72	6.52	0.69	4.76	0.64	4.27	0.63	3.82	0.62	2.89	0.62				
(17,1)	2685	9.03	0.82	7.19	0.79	5.25	0.73	4.70	0.72	4.21	0.70	3.19	0.70				
(19,1)	2925	9.83	0.91	7.83	0.88	5.72	0.81	5.12	0.80	4.59	0.79	3.48	0.78				

CHAPTER IV

DISCUSSION OF RESULTS

Membrane Characteristics. Two factors are required to obtain accurate values of modal surface density; a clearly defined asymptotic value of apparent membrane wave speed, and the ability to accurately measure resonant frequencies. Both conditions were fulfilled in this experiment.

Resonant Frequency Dampening. The accurate measurement of membrane dampening was recognized as one of the most difficult and most important aspects of this experiment. The 3 dB down values of dampening were selected for the calculation of ϕ_p . These values were selected because they were measured at the resonant frequency and resulted from the same excitation which produced the phenomena being measured. Although structural dampening played a much greater role in dampening than had been anticipated, the magnitude of the dampening, and not its source, is the significant parameter in this analysis. The high structural dampening observed is believed due to the elongated nature of the membrane, together with the low ($n=1$) transverse mode excited.

Response to Acoustic Excitation. Based on the observed data, it is believed that the membrane response to the low wave number component of pressure exceeds the

acoustic excitation response. No quantitative evaluation of their relative magnitudes can be made at this time. This is due to the limited data on flow induced acoustic levels in the wind tunnel test section, and a lack of knowledge as to modal orientation of this acoustic noise in the test section.

Pressure Spectral Density. The response contours of Figure 10 display the anticipated results that departure from the convective ridge is marked by a significant decrease in $\overline{\phi_p}$. Figure 10 also emphasizes the need to obtain more data on the distribution of the low wave number contribution. Note that the -81 dB isogram shown in Figure 9 corresponds to the "valley floor" of Figure 10.

CHAPTER V

CONCLUSIONS

The rectangular membrane is an effective low wave number filter.

The length to width ratio of the membrane used in this experiment to inhibit higher order transverse modes led to high structural dampening. This dampening, however, did not impair the membrane's usefulness above the lowest modes.

In the frequency and flow range where comparison is possible, the low wave number spectrum is greater than the response to wind tunnel acoustical excitation.

CHAPTER VI

RECOMMENDATIONS

Whereas the membrane has proven to be an effective low wave number filter, the data obtained in the course of these experiments has left unanswered some questions and has raised some previously unanticipated questions. To provide more definitive information on the contribution and significance of low wave number pressure fluctuations, additional experimentation will be required. It is believed that the following items are of primary importance in further analysis of the low wave number phenomena.

Obtain a wider range of data. It would be desirable to be able to experimentally determine the low wave number contribution continuously from the convective region downward. This would require lower membrane wave speeds, implying lower membrane tension.

Transform convective data. In order to compare the low wave number contribution to the convective contribution at low wave numbers, it is necessary to convert existing convective pressure spectral density information in the frequency domain to the wave number domain.

Extend evaluation of acoustic excitation. To fully assess the impact of wind tunnel induced acoustic excitation, wind tunnel acoustic data at varying flow rates must be determined. In addition, the acoustic pressure distri-

bution relative to the test section must be determined.

Analysis of higher order transverse modes. The analysis contained in Appendix I assumes negligible contribution from higher order transverse modes. The validity of this assumption should be verified, or the analysis modified to account for higher order transverse modes.

Analysis of transverse pressure coherence. A further constraint in the analysis of Appendix I specifies that both the membrane length and width be much greater than the transverse pressure coherence length. The transverse pressure coherence length, as determined by Blake (6), is on the same order as the membrane width. The effect of this phenomenon should be investigated.

Analytic prediction of added mass effects. Numerical integration of equation (3,1) by Davies (10) was attempted, but the results for the added mass effect were considered unreliable. An algorithm capable of accurately predicting both acoustic radiation dampening and added mass effects would be desirable. Specifically, accurate analysis of the added mass effect would indicate the accuracy of the membrane tension calculation.

REFERENCES

1. G. Maindanik and D.W. Jorgensen, "Boundary Wave-Vector Filters for the Study of the Pressure Field in a Turbulent Boundary Layer", Jour. Acous. Soc. Amer., 42, 2, pp 494-501, August 1967
2. W.K. Blake and D.M. Chase, "Wave Number Frequency Spectra of Turbulent Boundary Layer Pressure Measured by Microphone Arrays", Bolt, Beranek and Newman Report 1769, April 1969
3. P.W. Jameson, "Measurement of Low Wave Number Components of Turbulent Boundary Layer Wall Pressure Spectrum", Bolt, Beranek and Newman Report 1937, September 1970
4. F.A. Aupperle and R.F. Lambert, "On the Utilization of a Flexible Beam as a Spatial Filter", Jour. Sound and Vibr., 24, 2, pp 259-267, 1972
5. C.E. Hanson, "The Acoustics and Vibration Laboratory, Engineering Projects Laboratory", M.I.T., May, 1968
6. W.K. Blake, "Turbulent Boundary Layer Wall Pressure Fluctuations on Smooth and Rough Walls", Jour. Fluid Mech., 44, 4, pp 637 ff, December, 1970
7. T.E. Burton, "On the Generation of Wall Pressure Fluctuations for Turbulent Boundary Layers Over Rough Walls", M.I.T. Acoustics and Vibration Laboratory Report 70208-4, March, 1971
8. P. Leehey and H.G. Davies, "The Direct and Reverberant Response of Strings and Membranes to Convecting Random Pressure Fields", M.I.T. Acoustics and Vibration Laboratory Report 70208-8, 1973
9. P.M. Morse, Vibration and Sound. 2nd ed., pp 180, McGraw-Hill Book Company, 1948
10. H.G. Davies, "Acoustic Radiation from Fluid Loaded Rectangular Plates", M.I.T. Acoustics and Vibration Laboratory Report 71476-1, December 1969

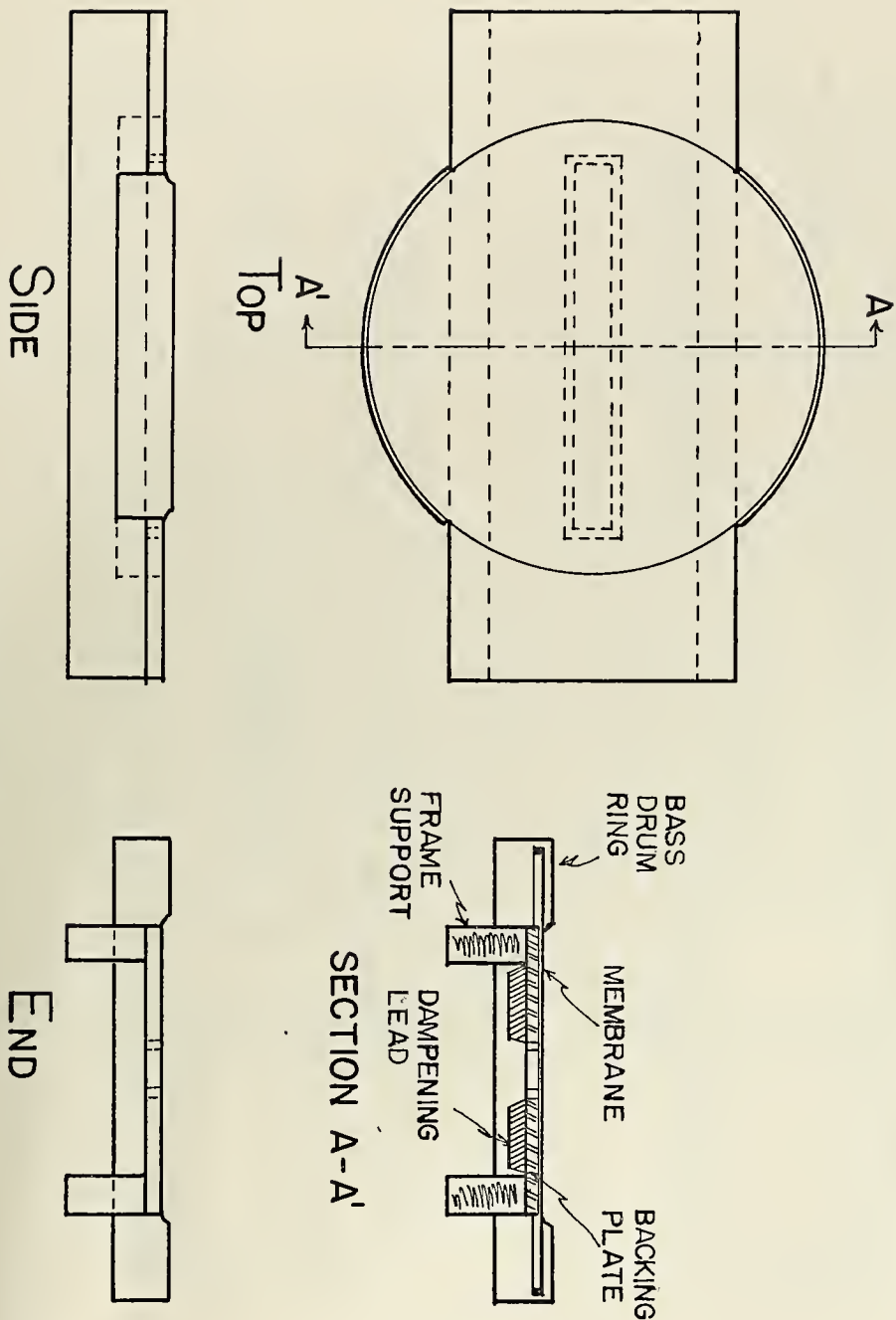


FIGURE 1-d

Membrane Support Mounting Detail

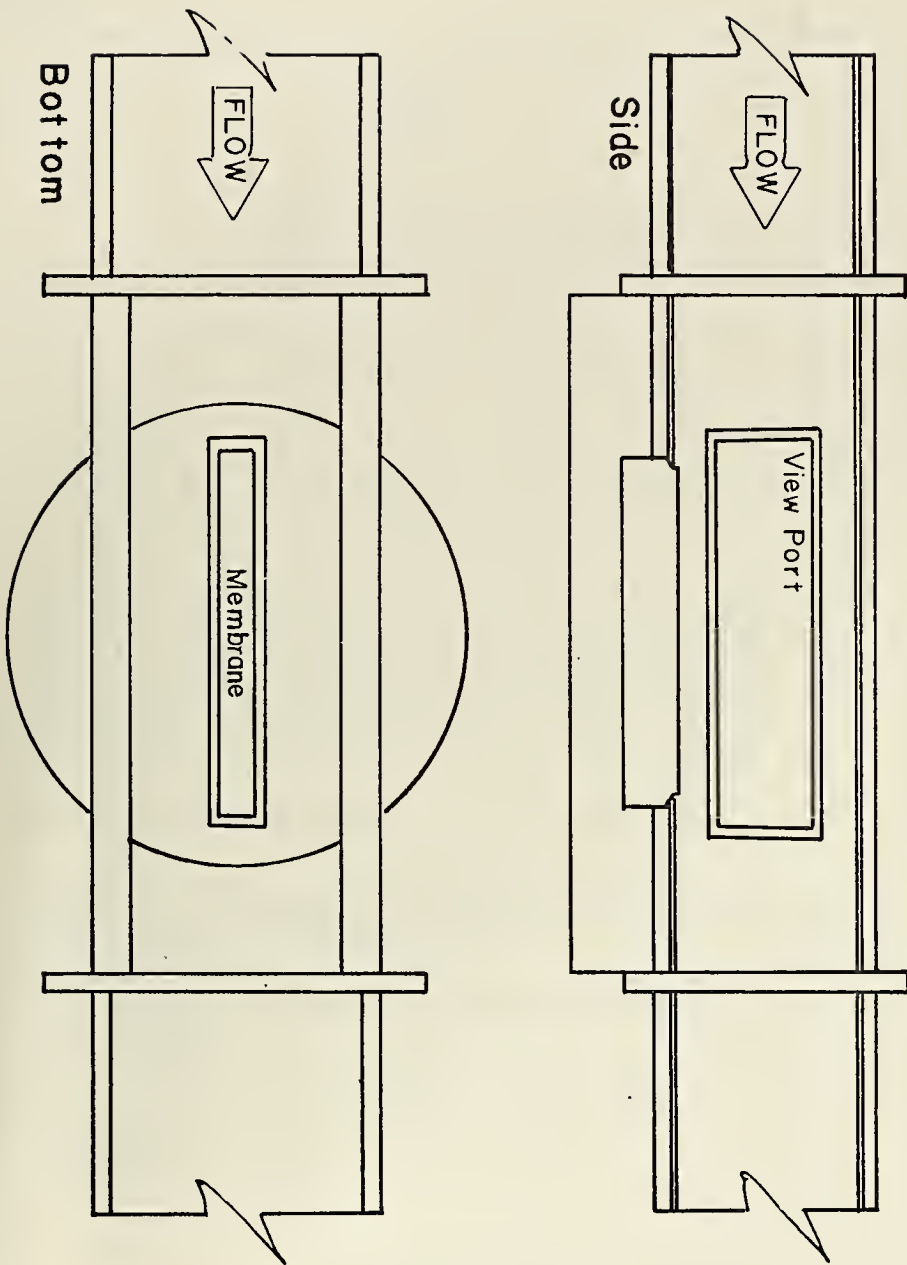
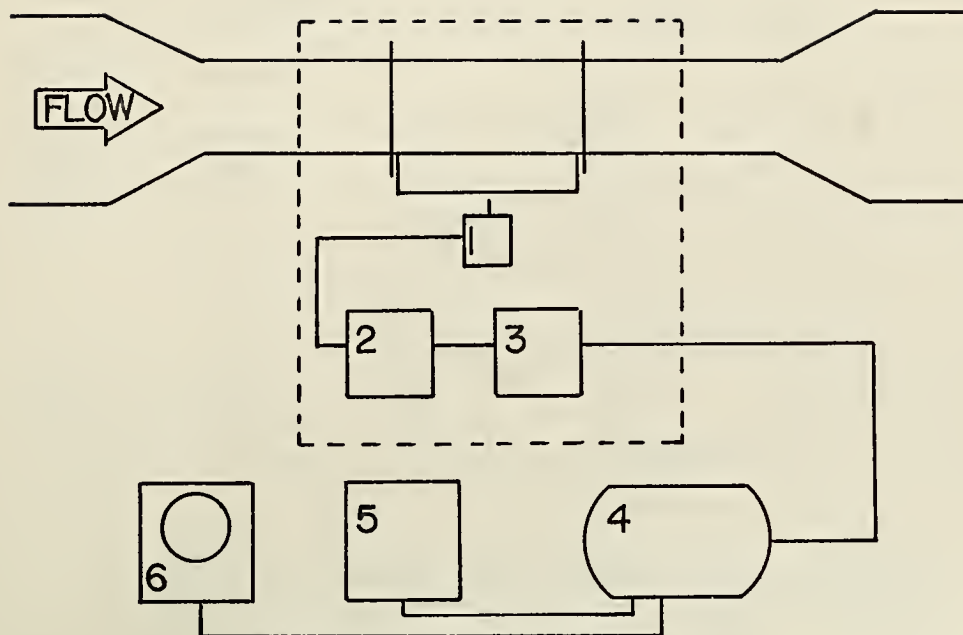


FIGURE 1-b

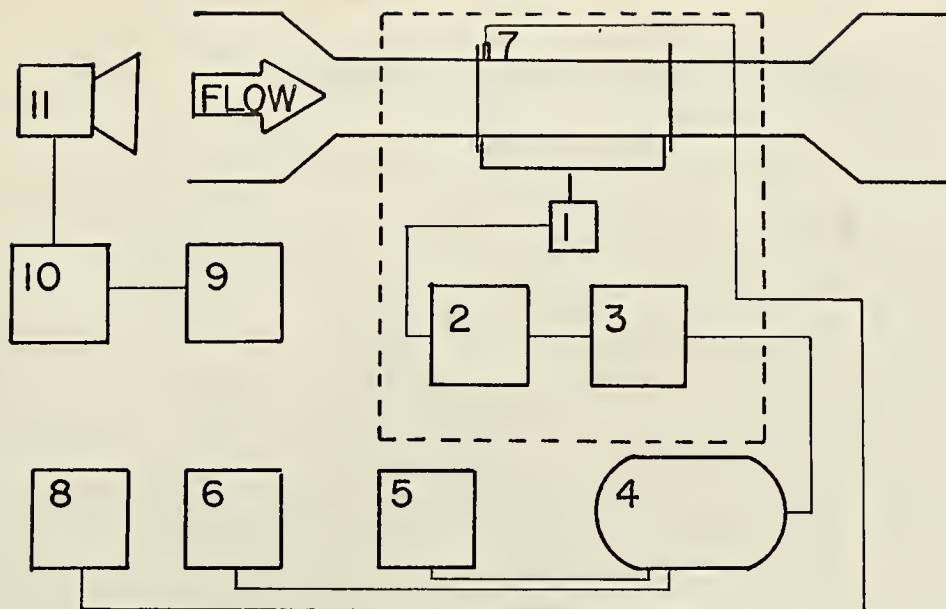
Membrane Wind Tunnel Mounting Detail



- 1 Optical Displacement Gage; Fotonic Sensor Model KD-3, Mechanical Technology, Inc.
- 2 Variable Band Pass Filter; Model 330 MR Krohn-Hite Corp.
- 3 Pre-Amplifier; Model 225, Ithaco Co.
- 4 Spectrum Analyzer/Averager; Model UA-15A/1015, Federal Scientific
- 5 X-Y Plotter; Mosley Autograph Model 135 L.M. Mosley Co.
- 6 Dual Beam Oscilloscope; Type 502A Tektronix, Inc.

FIGURE 2

Membrane Displacement Spectral Density
Measurement Equipment Schematic



- 1 Optical Displacement Gage; Fotonic Sensor Model KD-3, Mechanical Technology, Inc.
- 2 Variable Band Pass Filter; Model 330 MR Krohn-Hite Corporation
- 3 Pre-Amplifier; Model 225, Ithaco Co.
- 4 Spectrum Analyzer/Averager; Model UA-15A/1015, Federal Scientific
- 5 X-Y Plotter; Mosley Autograph Model 135 L.M. Mosley Co.
- 6 Dual Beam Oscilliscopes; Type 502A Tektronix, Incorporated
- 7 $\frac{1}{2}$ inch Condenser Microphone; B & K Instruments Incorporated
- 8 Frequency Analyzer; Type 2107, B & K Instruments, Incorporated
- 9 Random Noise Generator; Type 1402, B & K Instruments, Incorporated
- 10 Spectrum Shaper; Model 1612S2, B & K Instruments, Incorporated
- 11 Audio Amplifier and Driver

FIGURE 3

Membrane Acoustic Excitation Response
Measurement Equipment Schematic

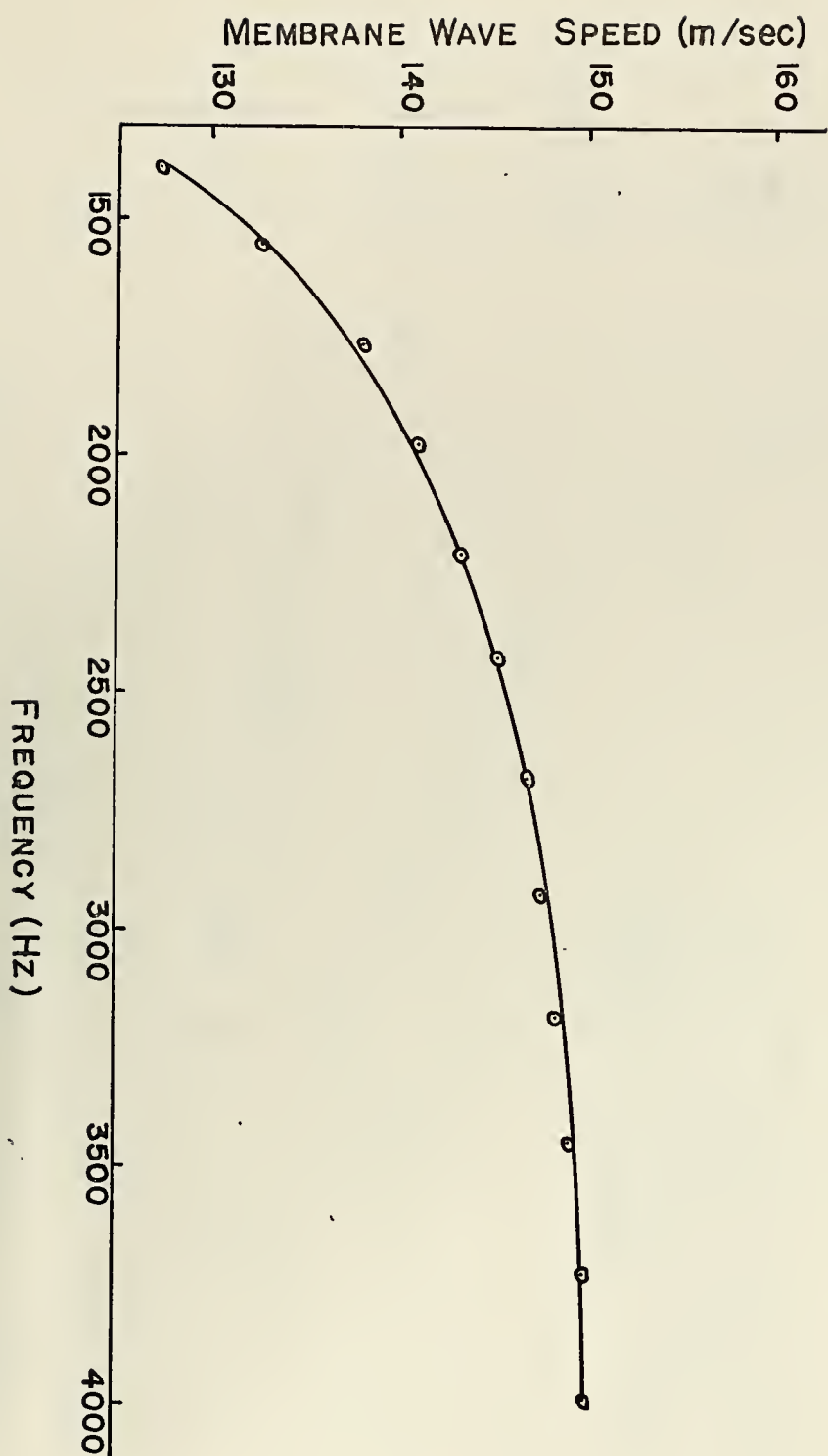


FIGURE 4

Apparent Membrane Wave Speed versus Frequency

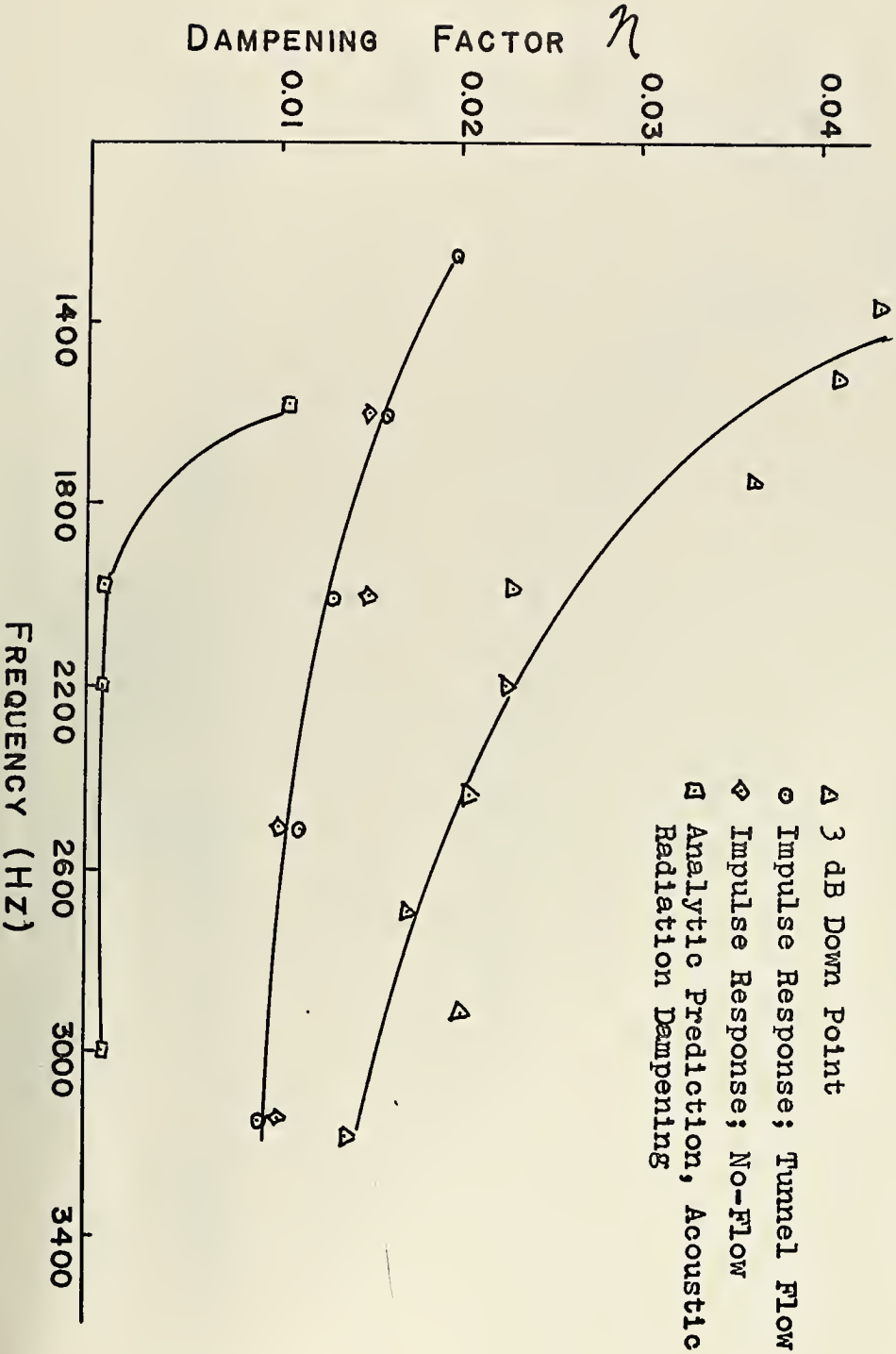


FIGURE 5

Membrane Dampening at Resonant Points

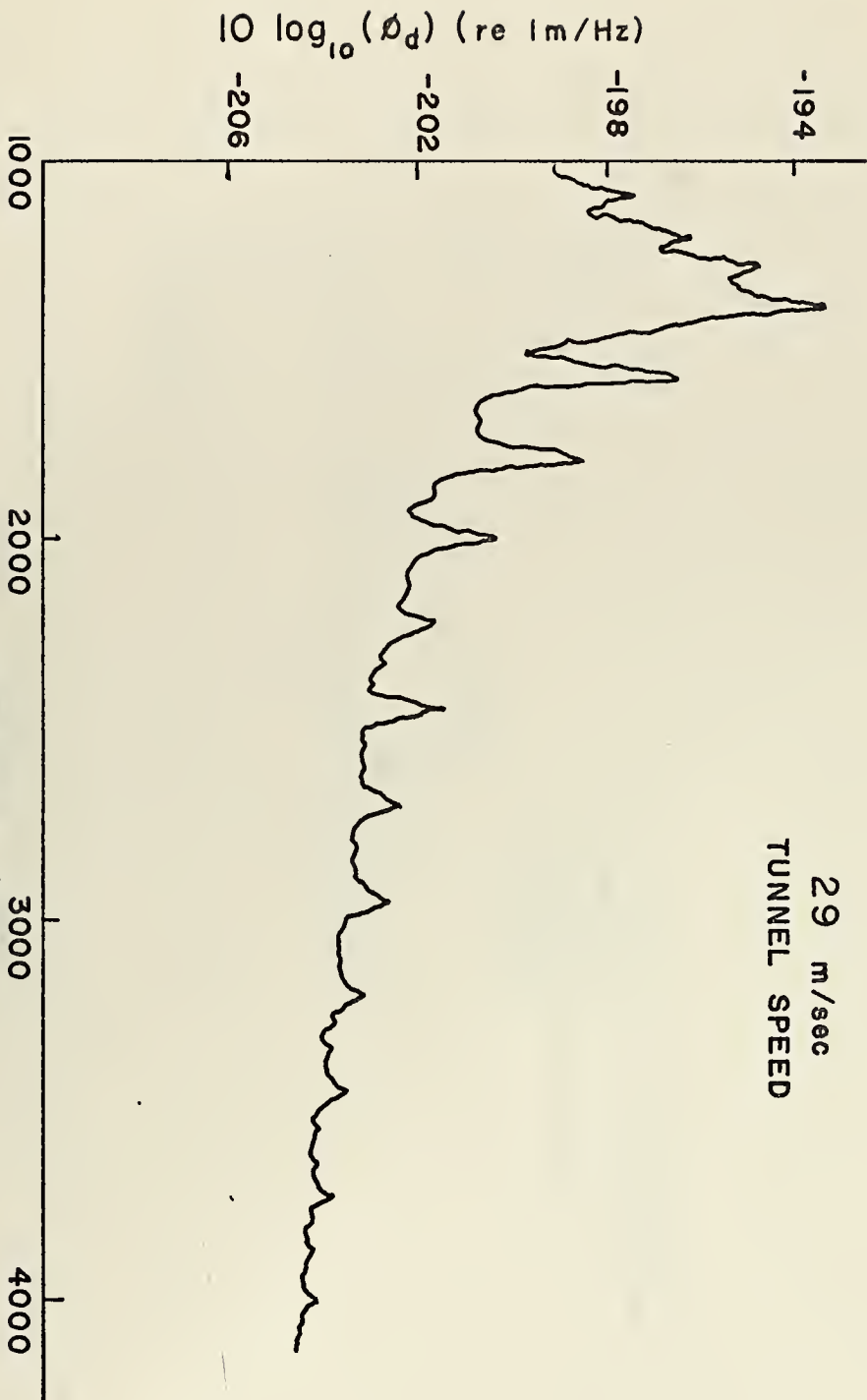


FIGURE 6

Membrane Displacement Spectral Density Response to
Plane Turbulent Boundary Layer Excitation

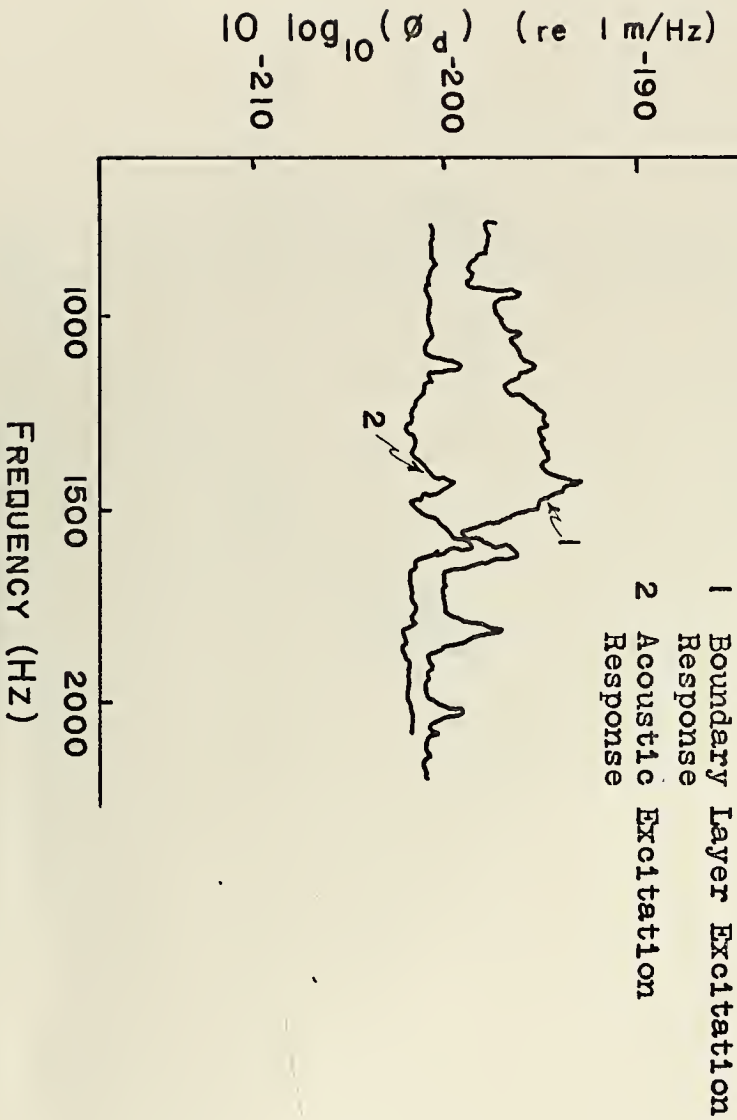


FIGURE 7

Membrane Displacement Spectral Density Response to Acoustic Excitation and Response to Plane Turbulent Boundary Layer Excitation

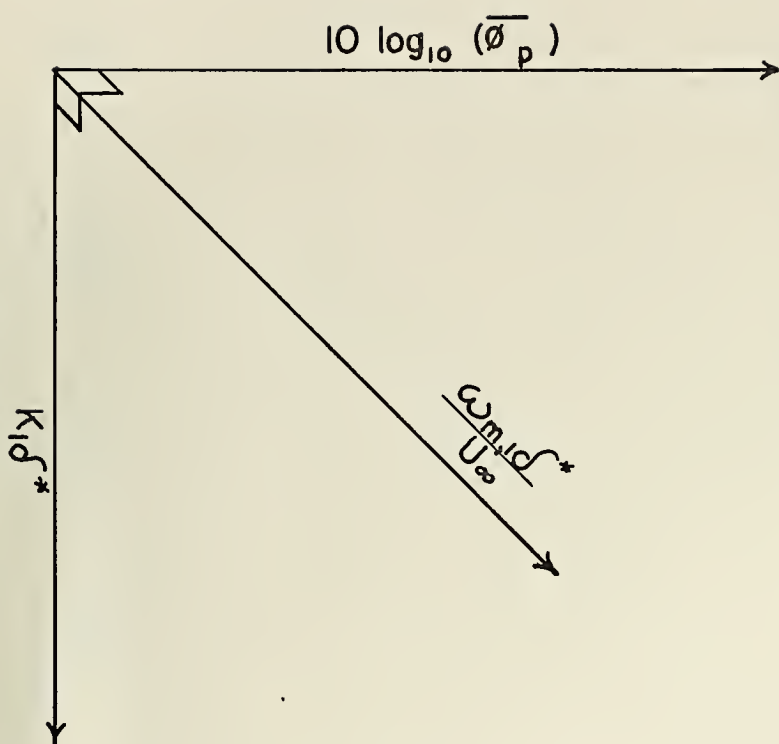


FIGURE 8

Data Coordinate System

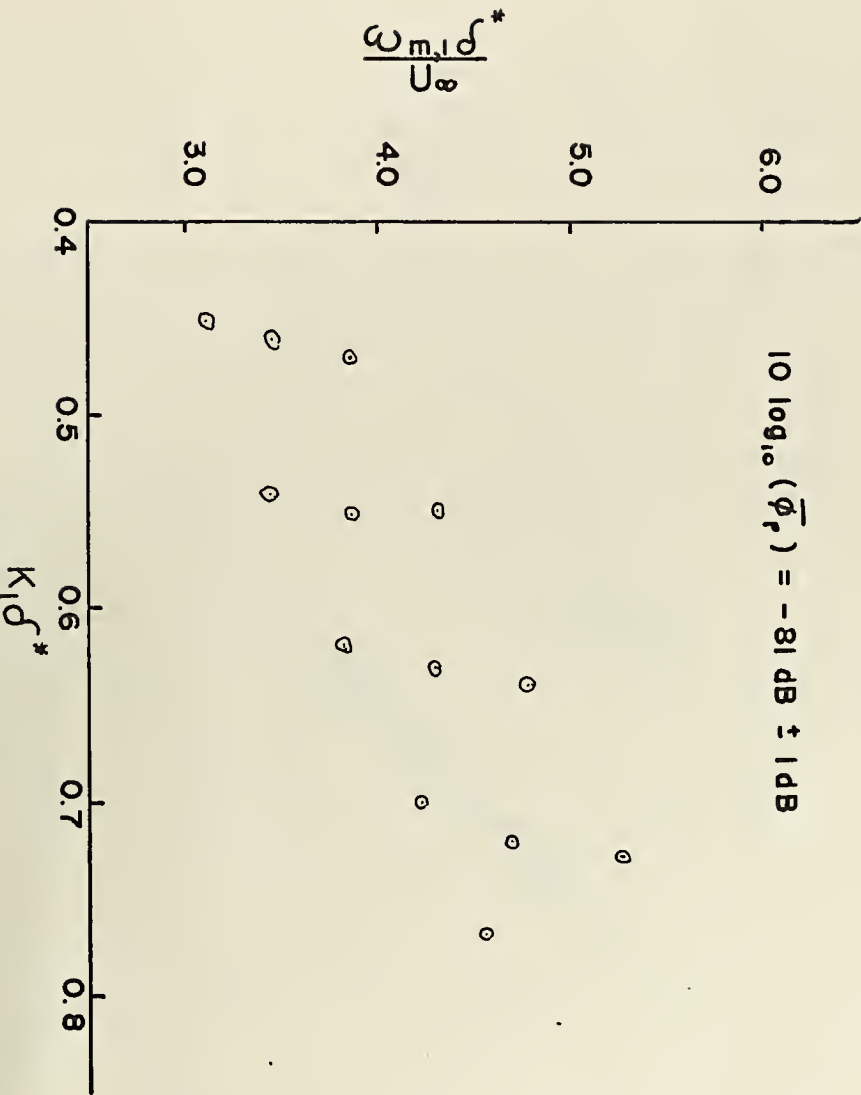
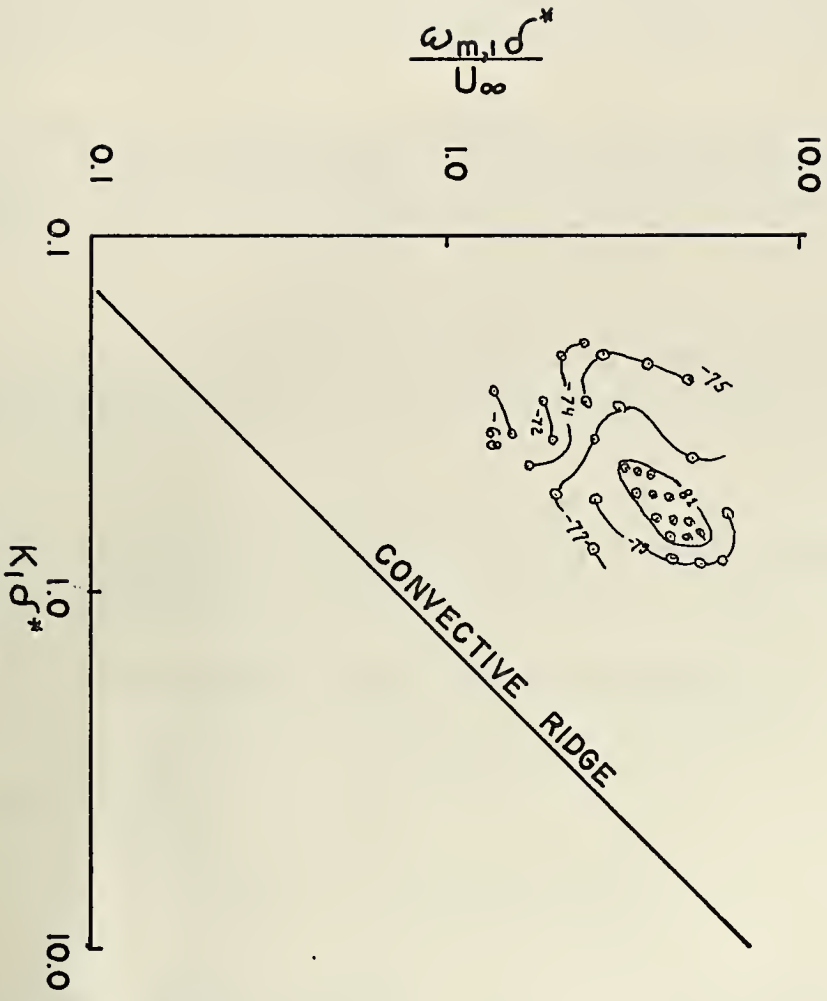


FIGURE 9

Low Wave Number Pressure
Spectral Density Isoogram



Low Wave Number Pressure Spectral Density
Response Contour

FIGURE 10

PERFORMANCE OF A MEMBRANE AS A
WAVE NUMBER FILTER

This analysis was performed by Professor Patrick Leehey. It is presented in appendix format because it has not been previously published and is requisite to an understanding of the transformation from displacement spectra to pressure spectra.

Consider a membrane of length l_1 and width l_3 installed flush in a plane rigid wall over which flows a turbulent boundary layer. The long dimension l_1 is aligned in the mean flow direction and it is required that

$$l_1 \gg l_3 \gg \lambda_3 \quad (\text{I-1})$$

where λ_3 is the lateral integral correlation length of the exciting wall pressure. From Leehey and Davies (8) it may be deduced that

$$\phi_d(\omega) = \frac{1}{(\sigma c^2)^2} \sum_{n=1}^{\infty} \sin^2\left(\frac{n\pi}{2}\right) \iint_{-\infty}^{\infty} |H_n(k_3)|^2 \left| C\left(\frac{l_1}{2}, k_1, k_n(\omega)\right) \right|^2 \phi_p(\bar{k}, \omega) d\bar{k} \quad (\text{I-2})$$

Here c is the membrane wave speed determined by

$$c^2 = T_m / \sigma \quad (\text{I-3})$$

The function

$$H_n(k_3) = \int_0^{l_3} e^{ik_3\eta} \sin\left[\frac{n\pi\eta}{l_3}\right] d\eta$$

is a lateral shape function. We have approximately in terms of Dirac- functions that

$$|H_n(k_3)|^2 \approx \frac{\pi l_3}{2} \left\{ \delta\left(k_3 - \frac{n\pi}{l_3}\right) + \delta\left(k_3 + \frac{n\pi}{l_3}\right) \right\}, \quad n > 1 \quad (\text{I-4a})$$

$$|H_n(k_3)|^2 \approx \pi l_3 \delta(k_3), \quad n = 0 \quad (\text{I-4b})$$

The function C is the k_1 -Fourier transform of the longitudinal factor of the membrane Green's function. Both can be expressed in closed form, for they are the same as for a string of length l_1 except for the term

$$K_n(\omega) = \left[\left(\frac{\omega}{c} \right)^2 - \left(\frac{n\pi}{l_3} \right)^2 - \frac{2i\beta\omega}{c^2} \right]^{\frac{1}{2}} \quad (\text{I-5})$$

$$\rightarrow \frac{\omega}{c} \quad \text{as } |\omega| \rightarrow \infty$$

with branch cut $|\text{Re } \omega| < \left[\left(\frac{n\pi c}{l_3} \right)^2 - \beta^2 \right]^{\frac{1}{2}}$, $\text{Im } \omega = \beta$, in the complex ω -plane. For small membrane damping β , and $\omega > \omega_n = \frac{n\pi c}{l_3}$

$$K_n(\omega) \approx \frac{\omega}{c} \left[1 - \left(\frac{\omega_n}{\omega} \right)^2 \right]^{\frac{1}{2}} - \frac{i\beta}{c} \left[1 - \left(\frac{\omega_n}{\omega} \right)^2 \right]^{-\frac{1}{2}} \quad (\text{I-5a})$$

but for $\omega < \omega_n$,

$$K_n(\omega) \approx \frac{\beta}{c} \left[\left(\frac{\omega_n}{\omega} \right)^2 - 1 \right]^{-\frac{1}{2}} - \frac{i\omega}{c} \left[\left(\frac{\omega_n}{\omega} \right)^2 - 1 \right]^{\frac{1}{2}} \quad (\text{I-5b})$$

from (I-4) we can write (I-2) as

$$\phi_d(\omega) = \frac{\pi l_3}{(\sigma c^2)^2} \left\{ \int_{-\infty}^{\infty} |C(\frac{l_1}{2}, k_1, K)|^2 \phi_p(k_1, 0, \omega) dk_1 \right. \quad (\text{I-6})$$

$$\left. + \frac{1}{2} \sum_{n=3,5,\dots}^{\infty} \int_{-\infty}^{\infty} |C(\frac{l_1}{2}, k_1, K_n)|^2 \left[\phi_p(k_1, \frac{n\pi}{l_3}, \omega) + \phi_p(k_1, -\frac{n\pi}{l_3}, \omega) \right] dk_1 \right\}$$

$$\left| C\left(\frac{l_1}{2}, k_1, K_n\right) \right|^2 = \frac{1}{|k_1^2 - k_n^2|^2} \left| 1 - \frac{\cos\left(\frac{k_1 l_1}{2}\right)}{\cos\left(\frac{k_n l_1}{2}\right)} \right|^2 \quad (\text{I-7})$$

The membrane resonant frequencies are given by ω_{mn} where

$$\omega_{m,n}^2 = \omega_m^2 + \omega_n^2, \quad \omega_m = \frac{m\pi c}{l_1}; \quad \omega_n = \frac{n\pi c}{l_3} \quad (\text{I-8})$$

Clearly resonant modal response can occur only for $\omega > \omega_n$. In particular, if we permit only the $n=1$ lateral mode component to contribute to resonant excitation, then only the first term on the right hand side of (I-6) is significant. By (I-5a) and (I-5b) we see that ω_n serves as a lateral modal cut-off frequency.

We can show that when (I-5a) applies, the wave number filter

$$\left| C\left(\frac{l_1}{2}, k_1, K_n(\omega_{m,n}) \right) \right|^2$$

has a band width

$$\Delta k_1 = \frac{2\pi}{l_1} \quad (\text{I-9})$$

for all odd m, n . In particular, we find for resonant frequencies

$$\omega_{m,1} = \frac{m\pi c}{l_1} \left[1 + \left(\frac{l_1}{m l_2} \right)^2 \right]^{\frac{1}{2}} \quad (\text{I-10})$$

that

$$\phi_d(\omega_{m,1}) = \frac{1}{2} \frac{l_3}{l_1} \left(\frac{\pi}{\sigma \beta \omega_{m,1}} \right)^2 \left[\phi_p\left(\frac{m\pi}{l_1}, 0, \omega_{m,1}\right) + \phi_p\left(-\frac{m\pi}{l_1}, 0, \omega_{m,1}\right) \right] \quad (\text{I-11})$$

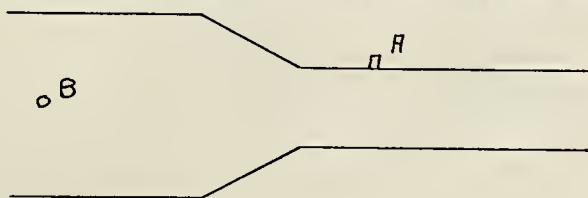
We can show that contributions of lateral modal components above the $n=1$ to $\phi_d(\omega_n)$ do not contain the large factor β^{-2} of (I-11) and hence, conforming to our earlier remark, may be neglected.

APPENDIX II

THE MEASUREMENT OF ACOUSTIC LEVELS
IN A WIND TUNNEL

This analysis was performed by Professor Patrick Leehey. It is presented in appendix format because it has not been previously published in this form and is requisite to an understanding of the membrane acoustic excitation portion of this experiment.

We assume the signal at B is acoustic and uncorrelated with turbulent boundary layer pressure fluctuations at A.



In narrow bands we have

$$B(t) = B \sin(\omega t + \psi) \quad (\text{II-1})$$

$$A(t) = a B \sin(\omega t + \psi + \phi) + A_T \sin(\omega t + \psi_T) \quad (\text{II-2})$$

Here B , ψ , A_T , ψ_T are independent random variables and ψ and ψ_T are uniformly distributed over $(0, 2\pi)$. The functions a and ϕ are deterministic functions of ω and depend on tunnel characteristics. A_T and ψ_T characterize the boundary layer pressure fluctuations at A, B and ψ characterize the acoustic interference pressure as seen at B.

$$\begin{aligned} C &= E A(t) B(t) = a E B^2 \sin(\omega t + \psi) \sin(\omega t + \psi + \phi) \\ &= a \cos \phi E B^2, \end{aligned} \quad (\text{II-3})$$

$$\begin{aligned} Q &= E A(t) B(t - \frac{\pi}{2}) = a E B^2 \sin(\omega t + \psi - \frac{\pi}{2}) \sin(\omega t + \psi + \phi) \\ &= -a \sin \phi E B^2 \end{aligned} \quad (\text{II-4})$$

Hence

$$|\Phi(\omega)|^2 = C^2 + Q^2 = [\alpha \mathcal{E} B^2]^2 \quad (\text{II-4})$$

Now

$$\Phi_B(\omega) = \mathcal{E} B^2(t) = \mathcal{E} B^2$$

$$\Phi_H(\omega) = \mathcal{E} H^2(t) = \alpha^2 \mathcal{E} B^2 + \mathcal{E} H_T^2$$

$$\stackrel{\text{a}}{=} \Phi_{\text{ACOUSTIC}}(\omega) + \Phi_{\text{TURBULENT}}(\omega) \text{ at } H \quad (\text{II-5})$$

$$\text{Then } \frac{|\Phi_{\text{RB}}(\omega)|^2}{\Phi(\omega)} = \alpha^2 \mathcal{E} B^2 = \Phi_{\text{ACOUSTIC}}(\omega) \text{ at } H \quad (\text{II-6})$$

Based on this analysis and wind tunnel characteristics, the acoustic levels at point "A" were measured by N.J. Spinka of the Acoustics and Vibration Laboratory. This data was converted to one-third octave average values to be compatible with the wave shaper and frequency analyzer shown in Figure 3.

APPENDIX III

NUMERICAL EVALUATION OF ϕ_p

From Equation (2):

$$\phi_d(\omega_{m,1}) = \left[\frac{1}{2} \left(\frac{l_3}{l_1} \right) \left(\frac{\pi}{\sigma_t \beta \omega_{m,1}} \right)^2 \right] \left[\phi_p(k_1, 0, \omega_{m,1}) + \phi_p(-k_1, 0, \omega_{m,1}) \right]$$

$$\phi_p(k_1, 0, \omega_{m,1}) + \phi_p(-k_1, 0, \omega_{m,1}) = \phi_d(\omega_{m,1}) \left[\frac{1}{2} \left(\frac{l_3}{l_1} \right) \left(\frac{\pi}{\sigma_t \eta \omega_{m,1}^2} \right)^2 \right]^{-1}$$

$$\phi_p(k_1, 0, \omega_{m,1}) + \phi_p(-k_1, 0, \omega_{m,1}) = \frac{1}{4\pi} \phi_d(F_{m,1}) \left[\frac{1}{2} \left(\frac{l_3}{l_1} \right) \left(\frac{\pi}{\sigma_t \eta \omega_{m,1}^2} \right)^2 \right]^{-1} \quad \text{(III-1)}$$

Equipment Characteristics:

Spectrum Analyzer/Averager

0 dB = 100 mv input level

Bandwidth = 16 Hz

Displacement Sensor response curve slope

10 μ in/mv

Preamplifier Gain

60 dB

Units Correction:

Spectrum Analyzer/Averager 0 dB output with respect to Displacement Sensor input (in meters).

$$C1 = 20 \log_{10} (100 \text{ mv}) \cdot (10 \mu\text{in/mv}) \cdot (1 \text{ in}/10^6 \mu\text{in})$$

$$X(1 \text{ m}/39.37 \text{ in})$$

$$C1 = -92 \text{ dB}$$

Displacement Spectral Density:

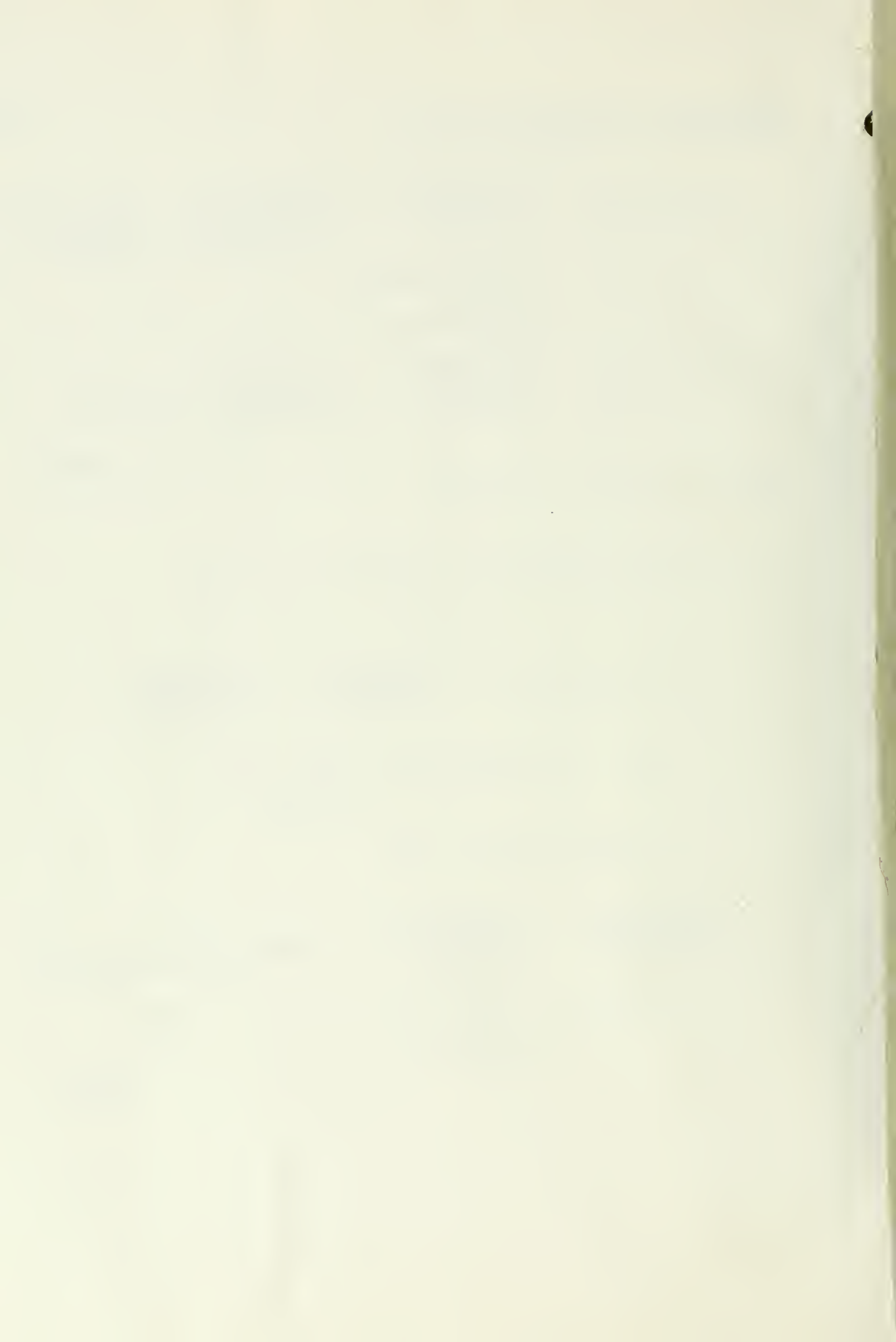
$$\begin{aligned}
 10 \log_{10}(\phi_d) &= \left[\begin{array}{l} \text{Analyzer/} \\ \text{Averager} \\ \text{Output} \end{array} \right] + \left[\begin{array}{l} \text{Band Width} \\ \text{Correction} \\ 10 \log_{10} \Delta f \end{array} \right] + \left[\begin{array}{l} \text{Analyzer/} \\ \text{Averager} \\ \text{Vernier} \end{array} \right] \\
 &+ \left[\begin{array}{l} \text{Preamplifier} \\ \text{Gain} \\ \text{Correction} \end{array} \right] + C1 \\
 10 \log_{10}(\phi_d) &= \left[\begin{array}{l} \text{Analyzer/} \\ \text{Averager} \\ \text{Output} \end{array} \right] + \left[\begin{array}{l} \text{Analyzer/} \\ \text{Averager} \\ \text{Vernier} \end{array} \right] - 164 \text{ dB}
 \end{aligned}$$

(III-2)

Combining (III-1) and (III-2):

$$\begin{aligned}
 10 \log_{10} \left\{ \frac{\phi_p(k_1, 0, \omega) + \phi_p(-k_1, 0, \omega) \cdot U_\infty}{q^2 \cdot \delta^* 2} \right\} &= \\
 10 \log_{10}(1/4 \pi) + \left[\begin{array}{l} \text{Analyzer/} \\ \text{Averager} \\ \text{Output} \end{array} \right] + \left[\begin{array}{l} \text{Analyzer/} \\ \text{Averager} \\ \text{Vernier} \end{array} \right] \\
 - 164 - 10 \log_{10} \left\{ \frac{1}{2} \frac{13}{11} \left(\frac{\pi}{\sigma_t \eta \omega_{m,1}^2} \right)^2 \right\} \\
 + 10 \log_{10} (U_\infty / q^2 \cdot \delta^* 2) \\
 = \left[\begin{array}{l} \text{Analyzer/} \\ \text{Averager} \\ \text{Output} \end{array} \right] + \left[\begin{array}{l} \text{Analyzer/} \\ \text{Averager} \\ \text{Vernier} \end{array} \right] - 10 \log_{10} \left\{ \frac{1}{2} \frac{13}{11} \left(\frac{\pi}{\sigma_t \eta \omega_{m,1}^2} \right)^2 \right\} \\
 + 10 \log_{10} \left[\frac{U_\infty}{q^2 \delta^* 2} \right] - 175
 \end{aligned}$$

(III-3)



Thesis
M8237

Morris

Measurement of low
wave number components
of wall pressure beneath
a plane turbulent bound-
ary layer.

145610

16 OCT 73

DISPLAY

Thesis
M8237

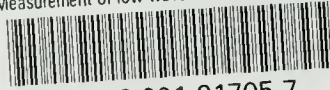
Morris

Measurement of low
wave number components
of wall pressure beneath
a plane turbulent bound-
ary layer.

145610

thesM8237

Measurement of low wave number component



3 2768 001 91705 7
DUDLEY KNOX LIBRARY